Extreme-ultraviolet absorption spectrum of Ga^+

P. Dunne, G. O'Sullivan, and V. K. Ivanov*
Physics Department, University College Dublin, Belfield, Dublin 4, Ireland
(Received 11 June 1993)

Time-resolved photoabsorption spectra of gallium plasmas have been photographed in the 50–450-Å region using the dual-laser-produced-plasma technique. The absorbing plasmas were produced by focusing the output of a *Q*-switched ruby laser onto slab targets while the background continuum was produced by focusing the output of a Nd:YAG oscillator-amplifier system (where Nd:YAG denotes neodymium-doped yttrium-aluminum-garnet) onto a samarium or hafnium target. At 130-ns delay between the two pulses the spectrum recorded was due almost exclusively to Ga^+. We have observed transitions due to both $3d$ and $3p$ excitation. In the former case we identified $3d^{10}4s^2$-$3d^9 4s^2 nf$ and $3d^9 4s^2 np$ series converging on the $^2D_{3/2}$ and $^2D_{5/2}$ limits of Ga^{2+}. In the $3p$ case no strong transitions were observed because of line broadening by super-Coster-Kronig decay of the $3p$ hole. The identifications were made by comparison with the predictions of Hartree-Fock and Dirac-Fock atomic-structure codes. Many-body calculations were also performed which proved invaluable in estimating the effects of different decay processes. The theoretical predictions are compared with the experimental data.

PACS number(s): 32.80.Hd, 32.30.Jc, 52.50.Jm

INTRODUCTION

The dual-laser-produced-plasma (DLPP) technique, in which one laser pulse is used to produce an intense background continuum while the second generates a plasma of the ions of interest, provides an ideal tool for the study of inner-shell photoabsorption of ions and refractory atoms. ([1–3], and references therein). The dominant ion stage in the absorbing plasma may be varied either by altering the laser-power density or the delay between the priming pulse and the backlighting continuum. Recombination in the plasma causes the average degree of ionization to fall rapidly with time, so that in general, increased time delays enable successively lower ion stages to be investigated.

In the present work we report the absorption spectrum of Ga^+ in the 50–450-Å region. The ground state of Ga^+ is Zn I–like, i.e., (Ne) $3s^2 3p^6 3d^{10} 4s^2$ and in the wavelength range investigated, discrete transitions and photoionization spectra due to $3p$ and $3d$ excitation are expected to occur. Very little work of a spectroscopic nature has been reported for such inner-shell excitation because of the difficulty in preparing an ion density sufficient for absorption studies. The $3d$ spectrum of neutral gallium was studied by Connerade [4] who found considerable interaction between channels for $3d$ and double-electron excitation in the $3d \rightarrow np$ Rydberg series for $n \geq 6$, the point which is coincident with the threshold for double-valence-electron photoionization. The isoelectronic Zn I subvalence spectrum by comparison, contains long and regular Rydberg series [5]. Valence-electron spectra of Ga^+ have been studied in detail by Isberg and Litzén [6] while precision energy-level and oscillator-strength calculations using accurate configuration-interaction wave functions for the resonance lines of the $n=4$ complex have been published by Tayal [7]. In the case of $3d$ and $3p$ excitation, absolute cross sections for electron-impact ionization have been deduced by Rogers *et al.* [8] by bombarding Ga^+ ion beams with electrons of variable energy and measuring the resulting production of doubly charged ions. They observed some resonance behavior of the differential cross section in the 20–35-eV region which they ascribed to $3d^9 4s^2 nl$ autoionization. More recently, absolute cross sections for electron-impact ionization in the 20–41-eV region with greatly enhanced energy resolution have been reported [9,10]. The strongest peaks were found at 21.88, 30.74, and 31.14 eV. The peak at 21.88 eV showed evidence of more than one component. In a theoretical investigation of electron-impact excitation followed by autoionization of the $3d^9 4s^2 4p$ configuration Pindzola, Griffin, and Bottcher [11] calculated for all 12 possible $3d^9 4s^2 4p$ final states. The dipole-allowed transitions $^1S_0 \rightarrow {}^3P_1$, $^1P_1$, and $^3D_1$ were predicted to have resonance energies of 21.9, 22.8, and 22.9 eV, and Rogers *et al.* [8] observed the more prominant structure in the $3d^{10}4s^2$-$3d^9 4s^2 4p$ cross section at 21.8, 22.4, and 23.5 eV. The peaks at 30.74 and 31.14 eV were ascribed by Peart and co-workers [9,10] to $3d^9 4s^2 5p$ autoionization and again the latter peak showed evidence of an additional weak feature close to 31.22 eV.

In this paper we report the observation of features due to $3d$ and $3p$ photoexcitation. Classifications are made by comparison with *ab initio* calculation and comparison made with previous photoelectron work.

EXPERIMENT

Two solid-state lasers were used to generate the plasmas. A 1.5-J 20-ns ruby pulse was focused to a line plasma of variable length to form the absorbing column of gallium ions. A 1-J 12-ns Nd:YAG laser pulse was focused onto a samarium or hafnium target at a time delay of between 10 and 200 ns. With the exception of some

*Present address: St. Petersburg State Technical University, Polytekhnicheskaya 29, St. Petersburg 195251, Russia.

modulation near 80 Å due to $4d$-$4f$ transitions, the spectrum of samarium is line free from 40 to 500 Å, while the hafnium spectrum is line free at wavelengths below 250 Å [12]. By varying the time delay between the plasmas, and by altering the length and hence the plasma temperature of the absorbing column, it was found that good separation of ion stages was obtainable.

The spectra were recorded on Kodak SWR plates mounted in a 2-m grazing-incidence spectrograph. Typically, 600 shots were needed to give adequate plate blackening. Analysis was carried out using calibrated traces from an optical microdensitometer and measurement from photographic enlargement. To provide reference lines, spectra of Al V through Al X, [13] generated by focusing the Nd:YAG output tightly onto an aluminum target, were superimposed on the absorption spectra. A cubic polynomial was fitted to the data and in all cases wavelength accuracy is better than 0.015 Å.

RESULTS

The Ga^+ spectrum obtained, reproduced in Fig. 1, was found to contain a number of strong absorption lines due to $3d^{10}4s^2 \rightarrow 3d^9 4s^2 nl$ excitation in the 300–450-Å region. At shorter wavelengths some structure due to $3p$ photoexcitation was also in evidence but this differed considerably from the Rydberg nature of the $3d$ spectrum. To help identify the lines multiconfiguration Dirac-Fock and Hartree-Fock with statistical exchange (HXR) calculations with the computer codes of Grant *et al.* [14], and Cowan [15,16] were performed on a VAX 11/780 computer. To interpret more completely the differences between the $3d$ and $3p$ spectra, calculations within the many-body-perturbation-theory framework [17] were also undertaken on a personal computer, using programs modified in accordance with the prescriptions of the automated system of atomic investigations [18,19]. The latter enabled linewidths to be calculated, and quantified the relative importance of autoionization and Auger decay mechanisms. To facilitate the discussion the $3d$ and $3p$ results are dealt with separately in what follows.

$3d$ PHOTOABSORPTION SPECTRUM

The $3d$ photoabsorption spectrum gives rise to a number of intense features in the 300–450 Å region. The ground state of Ga^+ is $(Ne)3s^2 3p^6 3d^{10} 4s^2\ ^1S_0$ and strong dipole-allowed transitions are expected to $(Ne)3s^2 3p^6 3d^9 4s^2 np, mf$ levels. As with the analogous Zn I spectrum [5], the resulting Rydberg series converging on the $3d^9(^2D_{3/2}, ^2D_{5/2})4s^2$ levels of Ga^{2+} are regular and well defined (Fig. 1). It was possible to observe most of the allowed transitions up to $n=11$ and $m=8$. Past these values the series converging on the $^2D_{3/2}$ limit lies above the $3d^9 4s^2\ ^2D_{5/2}$ threshold and lines in this region are broadened and weakened by autoionization. The energies and eigenvector compositions of the observed levels are listed in Tables I and II, while in Table III the calculated transition energies, gf values, and linewidths are presented for comparison. It is seen that in each case, *ab initio*-multiconfiguration Dirac-Fock (MCDF) calculations underestimate the energy of $3d$-np transitions by approximately 2.1 eV. In the $3d$-nf case convergence difficulties were encountered. For the HXR calculations the corresponding discrepancy is approximately 1.4 eV in both cases and no convergence problems were experienced. Since in Ga^+ the nf wave functions are not expected to penetrate into the core because of the large repulsive centrifugal pseudopotential which they experience, the higher members should exhibit almost constant quantum defects and were used to determine the positions of the $^2D_{3/2}$ and $^2D_{5/2}$ limits. The values obtained were for the $^2D_{3/2}$ limit 37.104 eV, and for the $^2D_{5/2}$ limit 36.655 eV. From these the effective quantum numbers of both the p and f series were deduced and these are listed in Table II. Because the $3d^{10}4s^2 \rightarrow 3d^9 4s^2 4p$ transition

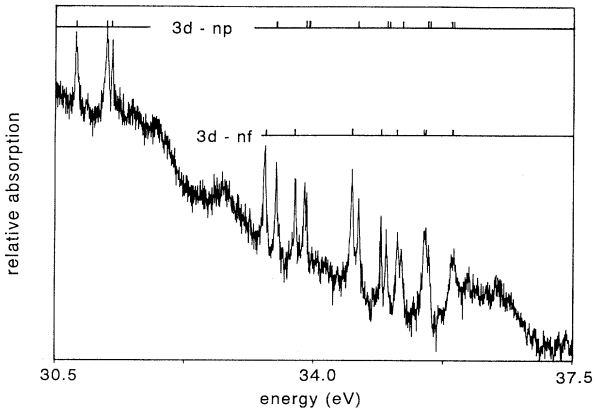

FIG. 1. Densitometer trace of the $3d^9$ photoabsorption spectrum of Ga^+.

TABLE I. Observed transitions in Ga^+ from the $3p^6 3d^{10} 4s^2(^1S_0)$ ground state.

Transition	λ (Å)	Energy (eV)
$3d_{5/2} \rightarrow 5p_{3/2}$	404.36	30.662
$3d_{3/2} \rightarrow 5p_{3/2}$	399.20	31.058
$3d_{3/2} \rightarrow 5p_{1/2}$	398.47	31.115
$3d_{5/2} \rightarrow 4f_{5/2,7/2}$	373.76	33.172
$3d_{5/2} \rightarrow 6p_{3/2}$	371.93	33.336
$3d_{3/2} \rightarrow 4f_{5/2}$	368.94	33.606
$3d_{3/2} \rightarrow 6p_{3/2}$	367.45	33.742
$\rightarrow 6p_{1/2}$	367.09	33.775
$3d_{5/2} \rightarrow 5f_{5/2,7/2}$	360.00	34.44
$3d_{5/2} \rightarrow 7p_{3/2}$	358.99	34.537
$3d_{3/2} \rightarrow 5f_{5/2}$	355.56	34.871
$3d_{3/2} \rightarrow 7p_{3/2}$	354.72	34.953
$\rightarrow 7p_{1/2}$	354.47	34.978
$3d_{5/2} \rightarrow 6f_{5/2,7/2}$	352.00	35.123
$4d_{5/2} \rightarrow 8p_{3/2}$	352.43	35.18
$3d_{5/2} \rightarrow 7f_{5/2,7/2}$	348.85	35.541
$3d_{3/2} \rightarrow 6f_{5/2}$	348.66	35.56
$3d_{5/2} \rightarrow 9p_{3/2}$	348.58	35.569
$3d_{3/2} \rightarrow 8p_{3/2,1/2}$	348.16	35.612
$3d_{5/2} \rightarrow 8f_{5/2,7/2}$	346.33	35.80
$3d_{5/2} \rightarrow 10p_{3/2}$	346.10	35.823
$3d_{3/2} \rightarrow 7f_{5/2}$	344.55	35.985
$3d_{5/2} \rightarrow 9f_{5/2,7/2}$	344.73	35.966
$3d_{5/2} \rightarrow 11p_{3/2}$	344.43	35.997

TABLE II. Energy levels, eigenvector composition, and effective quantum numbers for the $3d \rightarrow np, mf$ Rydberg series in Ga^+. Note: underlined values denote negative eigenvector components.

Level	n^*	%JJ composition	%LS composition
Series $3d_{3/2} \rightarrow np_{1/2}$			
$5p_{1/2}$	3.000	63%($\frac{1}{2}$) 37%($\frac{3}{2}$)	91% $^3D_1$ 8% $^1P_1$
$6p_{1/2}$	4.024	64%($\frac{1}{2}$) 36%($\frac{3}{2}$)	90% $^3D_1$ 9% $^1P_1$
$7p_{1/2}$	5.031	64%($\frac{1}{2}$) 36%($\frac{3}{2}$)	89% $^3D_1$ 9% $^1P_1$
$8p_{1/2}$	6.041	64%($\frac{1}{2}$) 36%($\frac{3}{2}$)	89% $^3D_1$ 9% $^1P_1$
Series $3d_{3/2} \rightarrow np_{3/2}$			
$5p_{3/2}$	3.015	59%($\frac{3}{2}$) 36%($\frac{1}{2}$)	51% $^1P_1$ 47% $^3P_1$
$6p_{3/2}$	4.044	63%($\frac{3}{2}$) 36%($\frac{1}{2}$)	61% $^3P_1$ 38% $^1P_1$
$7p_{3/2}$	5.060	64%($\frac{3}{2}$) 36%($\frac{1}{2}$)	65% $^3P_1$ 34% $^1P_1$
$8p_{3/2}$	6.041	64%($\frac{3}{2}$) 36%($\frac{1}{2}$)	64% $^3P_1$ 31% $^1P_1$
Series $3d_{5/2} \rightarrow np_{3/2}$			
$5p_{3/2}$	3.014	95%($\frac{3}{2}$)	51% $^3P_1$ 41% $^1P_1$
$6p_{3/2}$	4.050	99%($\frac{3}{2}$)	53% $^1P_1$ 38% $^3P_1$
$7p_{3/2}$	5.070	100%($\frac{3}{2}$)	57% $^1P_1$ 33% $^3P_1$
$8p_{3/2}$	6.075	100%($\frac{3}{2}$)	58% $^1P_1$ 31% $^3P_1$
			10% $^3D_1$
$9p_{3/2}$	7.081	96%($\frac{3}{2}$)	56% $^1P_1$ 30% $^3P_1$
$10p_{3/2}$	8.090	100%($\frac{3}{2}$)	59% $^1P_1$ 30% $^3P_1$
			10% $^3D_1$
$11p_{3/2}$	9.098	54%($\frac{3}{2}$)	32% $^1P_1$ 17% $^3P_1$
		30% $9p$($\frac{3}{2}$,$\frac{3}{2}$)	32% $9p$ $^3P_1$
			14% $9p$ $^1P_1$
Series $3d_{3/2} \rightarrow nf_{5/2}$			
$4f_{5/2}$	3.945	100%($\frac{5}{2}$)	41% $^3D_1$ 39% $^1P_1$
			19% $^3P_1$
$5f_{5/2}$	4.937	100%($\frac{5}{2}$)	40% $^3D_1$ 40% $^1P_1$
			20% $^3P_1$
$6f_{5/2}$	5.936	99%($\frac{5}{2}$)	40% $^3D_1$ 40% $^1P_1$
			20% $^3P_1$
$7f_{5/2}$	6.975	100%($\frac{5}{2}$)	40% $^3D_1$ 40% $^1P_1$
			20% $^3P_1$
Series $3d_{5/2} \rightarrow nf_{5/2,7/2}$			
$4f_{5/2,7/2}$	3.953	60%($\frac{5}{2}$) 40%($\frac{7}{2}$)	75% $^3P_1$ 22% $^1P_1$
		60%($\frac{7}{2}$) 40%($\frac{5}{2}$)	57% $^3D_1$ 38% $^1P_1$
$5f_{5/2,7/2}$	4.957	52%($\frac{5}{2}$) 48%($\frac{7}{2}$)	78% $^3P_1$ 18% $^1P_1$
		52%($\frac{7}{2}$) 48%($\frac{5}{2}$)	56% $^3D_1$ 42% $^1P_1$
$6f_{5/2,7/2}$	5.961	52%($\frac{5}{2}$) 48%($\frac{7}{2}$)	79% $^3P_1$ 16% $^1P_1$
		52%($\frac{7}{2}$) 48%($\frac{5}{2}$)	55% $^3D_1$ 44% $^1P_1$
$7f_{5/2,7/2}$	6.988	56%($\frac{5}{2}$) 44%($\frac{7}{2}$)	79% $^3P_1$ 14% $^1P_1$
		56%($\frac{7}{2}$) 44%($\frac{5}{2}$)	54% $^3D_1$ 46% $^1P_1$
$8f_{5/2,7/2}$	7.980	56%($\frac{5}{2}$) 44%($\frac{7}{2}$)	79% $^3P_1$ 14% $^1P_1$
		56%($\frac{7}{2}$) 44%($\frac{5}{2}$)	53% $^3D_1$ 46% $^1P_1$
$9f_{5/2,7/2}$	8.890	55%($\frac{5}{2}$) 44%($\frac{7}{2}$)	79% $^3P_1$ 14% $^1P_1$
		55%($\frac{7}{2}$) 45%($\frac{5}{2}$)	54% $^3D_1$ 46% $^1P_1$

lies outside the wavelength range accessible on our system it was possible only to make comparison with the $3d^{10}4s^2 \rightarrow 3d^9 4s^2 5p$ photoelectron data. Peart and coworkers [9,10] found peaks at 30.662, 31.058, and 31.115 eV, which, if a slight constant energy shift is allowed for, are in excellent agreement with our data.

For the many-body calculations the starting point was the execution of nonrelativistic random-phase-approximation exchange (RPAE) calculations which used single-electron Hartree-Fock (HF) wave functions as a zero-order basis. From these calculations energy position, corrected energy position, oscillator strengths, and autoionization widths due to interaction with valence electrons and decay to the $3d^{10}4s\epsilon p$ continuum were deduced. The next step was to determine the energy splittings and energy shift for ground and excited states and these values are included in the data of Table III. To obtain the cross section in the resonance region the RPAE procedure for spin-orbit-split $3d$ subshells was used and the five-channel interaction $4s^2 \rightarrow 4s\epsilon p$, $3d_{3/2,5/2}$-$np\epsilon p$, and $3d_{3/2,5/2} \rightarrow nf\epsilon f$ included. The $3d$ energy shift was then evaluated from the equation

$$E_{nl} - E_{nl}^{\mathrm{HF}} - \mathrm{Re}\langle nl \left| \sum (E_{nl}) \right| nl \rangle = 0 \ , \qquad (1)$$

where the summed terms represent the self-energy calculated from second-order perturbation theory for the nl hole in question. In the present case the self-energy of the $3d$ hole is represented by the following diagrams:

TABLE III. Energies, gf values, and widths of the $3d^{10}4s^2(^1S_0) \rightarrow 3d^9 4s^2 np, nf$ transitions in Ga^+. Note: E_{sp} refers to level splitting. Numbers in brackets indicate powers of ten.

Transition	E_{obs} (eV)	E_{DF} (eV)	E_{Cowan} (eV)	gf	E_{mb} (eV)	gf_{mb}	γ_{mb} (eV)
$3d_{5/2} \rightarrow 4p_{3/2}$		19.136	19.265	9.8[−3]	19.04		
$3d_{3/2} \rightarrow 4p_{3/2}$		20.019	20.206	4.0[−1]	19.49	0.544	0.063
$\rightarrow 4p_{1/2}$		20.105	20.262	1.5[−2]	$E_{sp}=0.2$		
$3d_{5/2} \rightarrow 5p_{3/2}$	30.662	28.477	29.208	1.5[−2]	28.84		
$3d_{3/2} \rightarrow 5p_{3/2}$	31.058	28.884	29.594	3.0[−2]	29.29	0.478	0.0029
$\rightarrow 5p_{1/2}$	31.115	28.964	29.677	4.9[−3]	$E_{sp}=0.038$		
$3d_{5/2} \rightarrow 6p_{3/2}$	33.336	31.105	31.914	1.2[−2]	31.45		
$3d_{3/2} \rightarrow 6p_{3/2}$	33.742	31.443	32.290	8.5[−3]	31.89	0.0192	9.5[−4]
$6p_{1/2}$	33.775	31.477	32.326	2.1[−3]	$E_{sp}=0.016$		
$3d_{5/2} \rightarrow 7p_{3/2}$	34.541	32.172	33.078	6.9[−3]	32.63		
$3d_{3/2} \rightarrow 7p_{3/2}$	34.953	32.613	33.495	3.5[−3]	33.08	0.0095	3.5[−4]
$\rightarrow 7p_{1/2}$	34.978	32.630	33.513	1.1[−3]	$E_{sp}=0.0082$		
$3d_{5/2} \rightarrow 8p_{3/2}$	35.180	32.802	33.722	4.5[−3]	33.28		
$3d_{3/2} \rightarrow 8p_{3/2}$	35.612	33.249	34.147	3.4[−3]	33.74	0.0055	1.9[−4]
$\rightarrow 8p_{1/2}$		33.359	34.156	6[−4]	$E_{sp}=0.0048$		
$3d_{5/2} \rightarrow 9p_{3/2}$	35.569	33.184	34.109	2.0[−3]			
$3d_{3/2} \rightarrow 9p_{3/2}$		33.634	34.541	2.9[−3]			
$\rightarrow 9p_{1/2}$		33.640	34.543	3[−4]			
$3d_{5/2} \rightarrow 10p_{3/2}$	35.823	33.433	34.363	1.7[−3]			
$3d_{3/2} \rightarrow 10p_{3/2}$		33.885	34.792	1.3[−3]			
$10p_{1/2} \rightarrow 10p_{1/2}$		33.890	34.796				
$3d_{5/2} \rightarrow 11p_{3/2}$	35.997	33.605	34.533	0			
$3d_{3/2} \rightarrow 11p_{3/2}$		34.060	34.967	9[−4]			
$11p_{1/2} \rightarrow 11p_{1/2}$		34.060	34.969				
$3d_{5/2} \rightarrow 4f_{5/2,7/2}$	33.172		31.673	8.9[−3]			
					31.31		
					$E_{sp}=0.000\,01$	0.0105	3.1[−4]
$3d_{3/2} \rightarrow 4f_{5/2}$	33.606		32.108	6.2[−3]	31.76		
$3d_{5/2} \rightarrow 5f_{5/2,7/2}$	34.440		32.956	6.6[−3]	32.55	0.0086	1.9[−4]
$3d_{3/2} \rightarrow 5f_{5/2}$	34.871		33.390	4.5[−3]	33.00		
$3d_{5/2} \rightarrow 6f_{5/2,7/2}$	35.123		33.648	4.5[−3]	33.23	0.0061	1.4[−4]
$3d_{3/2} \rightarrow 6f_{3/2}$	35.56		34.064	2.8[−3]	33.68		
$3d_{5/2} \rightarrow 7f_{5/2,7/2}$	35.541		34.062	2.8[−3]	33.63		
$3d_{3/2} \rightarrow 7f_{5/2}$	35.985		34.495	2.0[−3]	34.08		
$3d_{5/2} \rightarrow 8f_{5/2,7/2}$	35.80		34.330	2.1[−3]	33.88		
$3d_{3/2} \rightarrow 8f_{5/2}$			34.763	1.5[−3]	34.33		
$3d_{5/2} \rightarrow 9f_{5/2,7/2}$	35.966		34.513	1.5[−3]			
$3d_{3/2} \rightarrow 9f_{5/2}$			34.946	1.1[−3]			

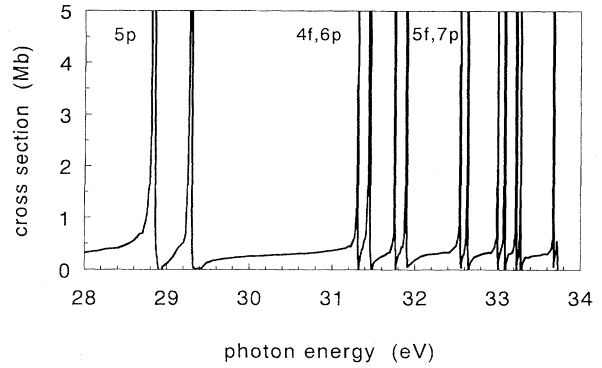

FIG. 2. 4*s* photoabsorption cross section of Ga^+ in the region of 3*d* excitation between 28 and 34 eV.

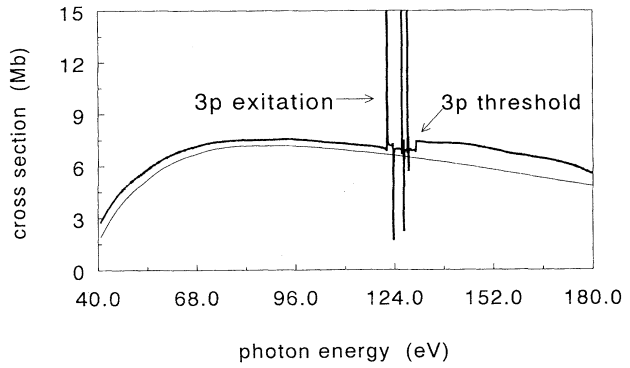

FIG. 3. 3*d* photoabsorption cross section of Ga^+ between 40 and 180 eV.

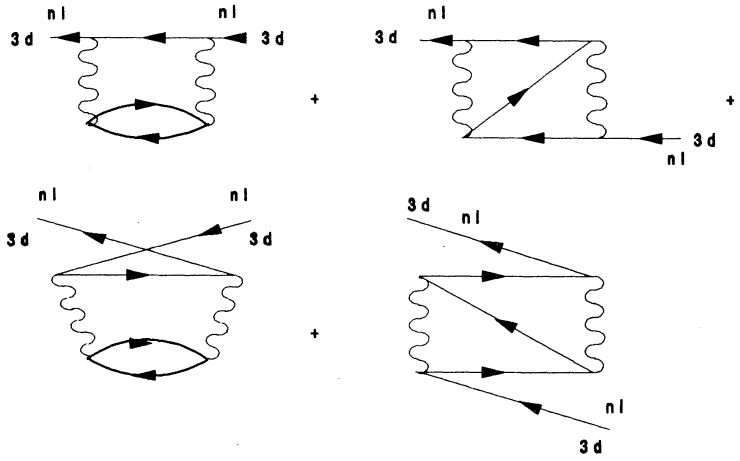

$$= \langle 3d \left| \sum (E_{3d}) \right| 3d \rangle \ , \qquad (2)$$

where the line with the arrow to the right (→) is the electron state and the line with the arrow to the left (←) is the HF hole state. The wavy line represents a Coulomb interaction. All values of transferred momentum from $L=0$ to 4 were included in these calculations. The value of the energy shift obtained was 5.75 eV and this value is incorporated in the data of Table III. The theoretical spectrum combining all these calculated values is presented in Fig. 2. It should be noted that the *np* or *mf* level splittings are not included in this figure as calculations showed that while the *np* splittings (at least for the lower *n* values) are sufficiently large to be observed experimentally, the *mf* splittings are not. The 3*d* continuum photoabsorption cross section in the energy region past 40 eV is reproduced in Fig. 3. In this region 3*d* photoionization is the dominant process and the 4*s* contribution is negligible by comparison. It should be noted that this figure was obtained from RPAE calculations where spin-orbit splitting was not accounted for. Also indicated here is the region of 3*p* excitation and the 3*p* threshold which will be dealt with in the next section.

3*p* PHOTOABSORPTION

In contrast to the 3*d* spectrum, no sharp lines were observed in the region below the 3*p* threshold. However some quite weak and broad absorption caused a small modulation of the transmitted continuum between 100 and 120 Å. An averaged densitometer trace, recorded from the same experiment as the 3*d* data, is presented in Fig. 4.

Calculations were performed using the HXR code of Cowan, RPAE method and many-body perturbation theory. The results of these calculations are presented in Table IV. It should be noted that, in general, the *gf* values obtained with the Cowan code are smaller than the corresponding values from the RPAE calculations (*gf* denotes the total oscillator strength, i.e., the absorption oscillator strength times the statistical weight of the final state). Also, a consistent shift $\Delta E = 6$ eV can be seen between the energy values from the Cowan code and those from the many-body perturbation calculations. The autoionizing widths obtained from the RPAE calculations are quite small, being of the order of 10^{-3} eV. From these data we could conclude that the excitations should give rise to well defined and visible spectral features. Comparison with the *gf* values presented for the 3*d* transitions in Table III emphasizes this point. The nonrelativistic theoretical spectrum for 3*p* excitation is presented in Fig. 5(a).

The data given in Table IV and Fig. 5(a) did not correlate with the observed spectrum, and so further many-body perturbation theory calculations were performed to

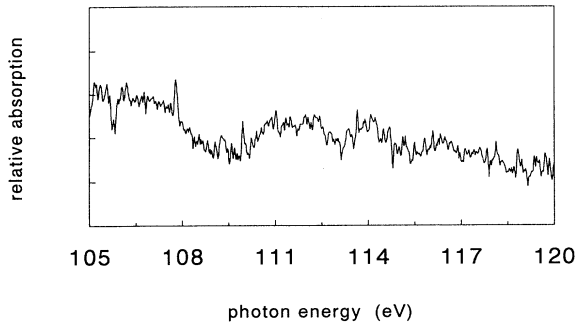

FIG. 4. Averaged densitometer trace of the $3p$ photoabsorption spectrum of Ga^+ showing $3p$-$5s$ excitation.

investigate the influence of $3p$-hole Auger decay on the spectrum. Auger decay can lead to a very significant broadening of spectral lines. Such line-broadening effects have already been discussed by Maguire [20] and Wendin and Ohno [21] in the case of $4p$ excitation in the elements around xenon. In Xe itself and the elements immediately preceding it, the one-electron-orbital picture of the $4p$ hole breaks down completely. The dominant process is a super-Coster-Kronig decay in which the $4p$ hole is filled by a transition from the $4d$ subshell, the excess energy from this transition enabling a further $4d \rightarrow \epsilon p \epsilon f$ excitation to occur.

Related though less dramatic behavior has been observed in the $3d$ photoabsorption spectrum of neutral copper [22]. Here discrete transitions of the type $3p^6 3d^{10} 4s \rightarrow 3p^5 3d^{10} 4sns, md$ are not observed and the spectrum is found to contain some broad weak features. These are due to spin-orbit-split $3p \rightarrow 4s$ transitions broadened by the width of the $3p$ hole, which was explained by Davis and Feldcamp [23] as arising from the super-Coster-Kronig decay $3p^5 3d^{10} 4snl \rightarrow 3p^6 3d^8 4snl\ \epsilon p \epsilon f$.

In the many-body calculations reported here the real and imaginary parts of the self energy of the $3p$ hole were obtained from second-order perturbation theory. [See Eq. (2).] The energy of the $3p$ hole is obtained as before from Eq. (1). The real part of the self-energy gives the energy

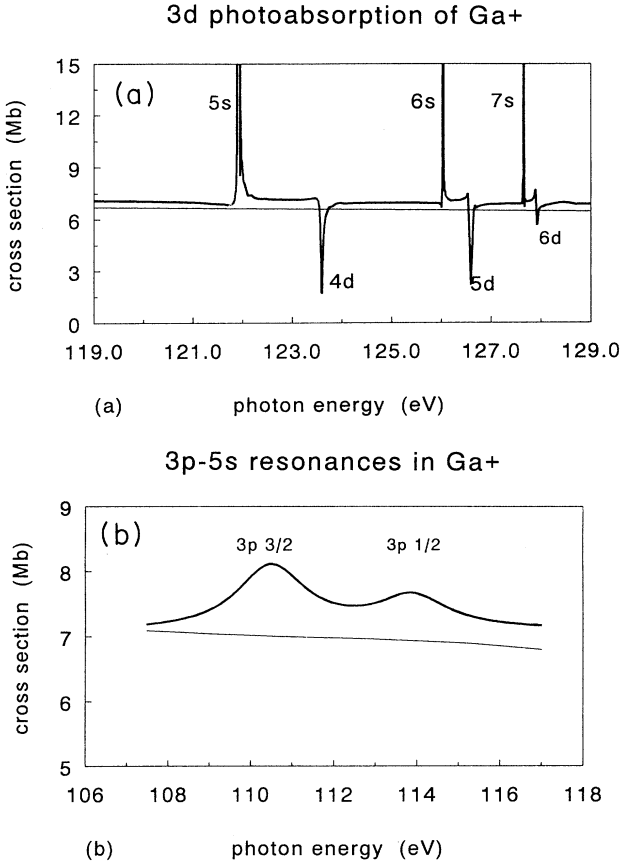

FIG. 5. (a) Nonrelativistic photoabsorption spectrum for $3p$ excitation in Ga^+, between 119 and 129 eV. (b) Calculated cross section for spin-orbit-split $3p$-$5s$ excitation in Ga^+ between 106 and 118 eV.

shift of the $3p$ hole ($=10.2$ eV) while the imaginary part yields the width of the hole due to Auger decay. The calculated energies with shift included are presented in Table IV.

The values for the spin-orbit splitting obtained with the Cowan code agree quite well with those from the many-body perturbation theory. The typical $3p$ splitting is

TABLE IV. Calculated energies, gf values, and widths of the $3d^6 3d^{10} 4s^2 ({}^1S_0) \rightarrow 3p^5 3d^{10} 4s^2\ ns, nd$ transitions in Ga^+. Numbers in brackets indicate powers of ten.

Transition	E_{Cowan} (eV)	gf_{Cowan}	E_{mb} (eV)	gf_{mb}	γ_{mb} (eV)
$3p_{3/2} \rightarrow 5s_{1/2}$	116.74	1.7[−2]	110.49	5.50[−2]	73.[−3]
$3p_{1/2} \rightarrow 5s_{1/2}$	120.22	8.5[−3]	113.87		
$3p_{3/2} \rightarrow 6s_{1/2}$	120.67	6.8[−3]	114.60	1.36[−2]	1.9[−3]
$3p_{1/2} \rightarrow 6s_{1/2}$	124.14	3.3[−3]	177.98		
$3p_{3/2} \rightarrow 7s_{1/2}$	122.25	3.1[−3]	116.21	6.02[−3]	8.5[−4]
$3p_{1/2} \rightarrow 7s_{1/2}$	125.75	1.6[−3]	119.59		
$3p_{3/2} \rightarrow 8s_{1/2}$	123.06	1.7[−3]	117.03	3.25[−3]	3.8[−4]
$3p_{1/2} \rightarrow 8s_{1/2}$	126.57	9.4[−4]	120.41		
$3p_{3/2} \rightarrow 4d_{3/2,5/2}$	118.07	1.3[−3]	112.18	3.77[−3]	4.8[−2]
$3p_{1/2} \rightarrow 4d_{3/2}$	121.63	8[−4]	115.56	3.77[−3]	4.8[−2]
$3p_{3/2} \rightarrow 5d_{3/2,5/2}$	121.18	8[−4]	115.16	1.53[−3]	1.8[−2]
$3p_{1/2} \rightarrow 5d_{3/2}$	124.69	4[−4]	118.54		
$3p_{3/2} \rightarrow 6d_{3/2,3/2}$	122.51	5[−4]	116.48	7.8[−4]	1.1[−2]
$3p_{1/2} \rightarrow 6d_{2/2}$	126.04	3[−4]	119.86		

found to be 3.4 eV. The partial widths for $3p$ decay via super-Coster-Kronig, Coster-Kronig, and usual Auger processes are given below.

$$\gamma_{\mathrm{SCK}}=1.71 \text{ eV} \quad 3p^5 3d^{10} 4s^2 nl \rightarrow 3p^6 3d^8 4s^2 ns\epsilon f \epsilon p \ ,$$

$$\gamma_{\mathrm{CK}}=0.26 \text{ eV} \quad \rightarrow 3p^6 3d^9 4s^1 ns\epsilon p \ ,$$

$$\gamma_{\mathrm{Auger}}=7.5E-6 \text{ eV} \quad \rightarrow 3p^6 3d^{10} ns\epsilon p \ .$$

The total width is 1.97 eV. It can be seen that the main contribution to the widths comes from super-Coster-Kronig decay.

The total widths are 3 orders of magnitude larger than the largest autoionizing widths presented in Table IV. Following a procedure similar to that of Davis and Feldcamp [23] the Fano formula was used to describe the cross section in the region of $3p \rightarrow 5s$ excitation. Using our calculated values for the widths, the parameters for the Fano formula were re-established. The cross section for the spin-orbit-split $5s$ excitation is presented in Fig. 5(b). The data presented in Fig. 4 were obtained from an averaging of four densitometer scans of different vertical regions of the photographic plate. It can be seen that the general agreement with the calculated cross section of Fig. 5(b) is quite good. Both the ratio of the $3p_{1/2}$ and $3p_{3/2}$ cross sections, and the splitting of the $3p$ hole are in good agreement with the theoretical estimations. Owing to the weakness of the other $3p$-ns features, and the moderate dynamic range of the plates, no further features could be identified with any degree of certainty.

CONCLUSION

We have observed $3p$ and $3d$ photoabsorption spectra of Ga^+. In the case of the $3d$ spectra well-developed regular Rydberg series are observed due to $3d$-np and $3d$-mf transitions. In the $3p$ case no such structure is observed because of the "melting" of the $3p$ hold by Auger processes. The DLPP technique has been shown to be very suitable for inner-shell photoabsorption studies and at present work on the $3p$ and $3d$ spectra of Cu^+, Ga^{2+}, and Ge^{2+} is ongoing.

ACKNOWLEDGMENTS

The authors wish to express their gratitude to Dr. A. A. Gribakina, Dr. G. F. Grabakin, and Cormac McGuinness for invaluable assistance with the many-body calculations. One of the authors (V.K.I.) wishes to express his gratitude for support from the U.C.D. President's Research Fund which permitted his visit to U.C.D. We also wish to thank Professor R. D. Cowan for sending us his computer codes, Professor P. K. Carroll for his interest in and enthusiasm for this work, and Dr. J. White and D. Cooney for their expertise in the design and construction of the target chamber used. The work was supported by the Irish Science and Technology Agency EOLAS under Research Grant No. SC-91-112 and the European Community under Grant No. SCI-0364.

[1] P. K. Carroll and E. T. Kennedy, Phys. Rev. Lett. **38**, 1068 (1977).
[2] J. T. Costello *et al.*, Phys. Scr. **T34**, 77 (1991).
[3] J. T. Costello *et al.*, J. Phys. B **25**, 5055 (1992).
[4] J. P. Connerade, Proc. R. Soc. London Ser. A **354**, 511 (1977).
[5] W. R. S. Garton and J. P. Connerade, Astrophys. J. **155**, 667 (1969).
[6] B. Isberg and U. Litzén, Phys. Scr. **31**, 533 (1985).
[7] S. S. Tayal, Phys. Scr. **43**, 270 (1991).
[8] W. T. Rogers *et al.*, Phys. Rev. A **25**, 737 (1982).
[9] B. Peart, C. Lyon, and K. Dolder, J. Phys. B **20**, 5403 (1987).
[10] B. Peart and J. Underwood, J. Phys. B **23**, 2343 (1990).
[11] M. S. Pindzola, D. C. Griffin, and C. Bottcher, Phys. Rev. A **25**, 211 (1982).
[12] R. L. Kelly, Oak Ridge National Laboratory Report No. 5922, 1982 (unpublished).
[13] P. K. Carroll and G. O'Sullivan, Phys. Rev. A **25**, 275 (1982).
[14] Grant *et al.*, Comput. Phys. Commun. **21**, 207 (1980).
[15] R. D. Cowan, *The Theory of Atomic Structure and Spectra* (University of California, Berkeley, 1981).
[16] R. D. Cowan, J. Opt. Soc. Am. **58**, 808 (1968); **58**, 924 (1968).
[17] M. Ya. Amusia, *Atomic Photoeffect* (Plenum, New York, 1990), Chaps. 4 and 7.
[18] M. Ya. Amusia and L. V. Chernysheva, *Automated System of Atomic Investigation* (Nauka, Leningrad, 1989), in Russian.
[19] G. F. Gribakin and A. A. Gribakina (private communication).
[20] E. Maguire, Phys. Rev. A **9**, 1840 (1974).
[21] G. Wendin and M. Ohno, Phys. Scr. **14**, 148 (1976).
[22] R. Bruhn, B. Sonntag, and H. W. Wolf, J. Phys. B **12**, 203 (1979).
[23] L. C. Davis and L. A. Feldcamp, Phys. Rev. A **24**, 1862 (1981).